

Thermoresistivity of Carbon Nanostructures and their Polymeric Nanocomposites

Francis Avilés

Carbon nanostructures such as carbon nanotubes, graphene, and its multi-layer derivatives exhibit temperature-dependent electrical conductivity. They can form percolated networks inside polymers, which render electrical conductivity to nanocomposites. Upon the formation of a percolated network, thermal energy applied to the material drives structural changes of the network, which manifest as changes in electrical conductivity. This principle is used to develop smart materials with self-sensing temperature capabilities. This critical review covers past and present research on the electrical response to temperature (thermoresistivity) of carbon nanostructures and their polymeric nanocomposites. It covers few- and multi-layer graphene, carbon nanotubes, carbon-nanostructured arrays and fibers (yarns). The mechanisms driving the thermoresistive response of individual nanostructures, their arrays, and of their polymeric nanocomposites are addressed. The role of the nanostructured filler on the thermoresistivity of polymer nanocomposites depends on its morphology and concentration. For low filler concentrations, thermal expansion of the polymer may dominate over the inherent thermoresistivity of the filler. For high filler concentrations, or for densely packed arrays of carbon nanostructures, the inherent (quantum) thermoresistive response of the nanostructures becomes dominant. The review addresses recent progress in the field, highlights current issues, synthesizes published data, and provides outlooks and insights into future directions.

because temperature increases electron scattering in the vibrating crystalline lattice.^[1] For semiconductors, on the other hand, the electrical conductivity is determined by the concentration of electrons and holes in the conduction (electrons) and valence (holes) bands, and such concentration increases with increased temperature. Thus, quantum mechanics principles predict that as temperature increases, the conductivity of a semiconductor increases (resistivity decreases) in an exponential fashion, because more charge carriers are available for conduction.^[2] Carbon nanostructures such as carbon nanotubes and few-layer graphene sheets can increase or decrease their electrical resistivity upon an increase in temperature, depending on their number of layers, electronic structure (metallic, semimetal, semiconductor), and functional groups, among other factors.^[3–5] When they are used as percolated fillers in polymer composites, the effective conductivity of the nanocomposite is a function of the electronic properties of the filler, their size, morphology, their state of dispersion, and the filler

concentration within the polymer. Therefore, by understanding and controlling the relationships among these factors, individual carbon nanostructures, arrays, fibers, yarns, and carbon-nanostructured polymer nanocomposites can be used to develop smart self-sensing materials. The applications are vast, ranging from temperature sensors,^[6,7] smart textiles,^[8] smart structural materials,^[9] to tailored materials aiming for temperature-independent resistance.^[4,10] **Figure 1.** In some applications, such as for the development of strain sensors, a zero-temperature coefficient of resistance is sought. This aims to isolate the effect of strain from that of temperature on the electrical resistance.^[4,10,11]

This review covers fundamental concepts, mechanisms, current issues, and critical discussions on the temperature-dependent electrical response (thermoresistivity) of carbon nanotubes, carbon-nanostructured arrays, carbon nanotube fibers and yarns, graphenic sheets, and their polymer composites. After a brief introduction (section #1), section #2 summarizes the fundamentals of thermoresistivity as a coupled phenomenon and the most common mechanisms reported for the materials covered herein. Section #3 focuses on the thermoresistive response of individual nanostructures, i.e., carbon

1. Introduction

The fact that the electrical conductivity (σ) of solid materials depends on temperature (T) is long-known. For pure metals, the electrical resistivity ($\rho = 1/\sigma$, the reciprocal of conductivity) typically increases linearly with increased temperature (T). This is

F. Avilés

Centro de Investigación Científica de Yucatán
 Unidad de Materiales

Calle 43 No.130 x32 y 34, Col. Chuburná de Hidalgo, Mérida, Yucatán
 97205, Mexico

E-mail: faviles@cicy.mx

 The ORCID identification number(s) for the author(s) of this article can be found under <https://doi.org/10.1002/admi.202300218>

© 2023 The Authors. Advanced Materials Interfaces published by Wiley-VCH GmbH. This is an open access article under the terms of the Creative Commons Attribution License, which permits use, distribution and reproduction in any medium, provided the original work is properly cited.

DOI: 10.1002/admi.202300218

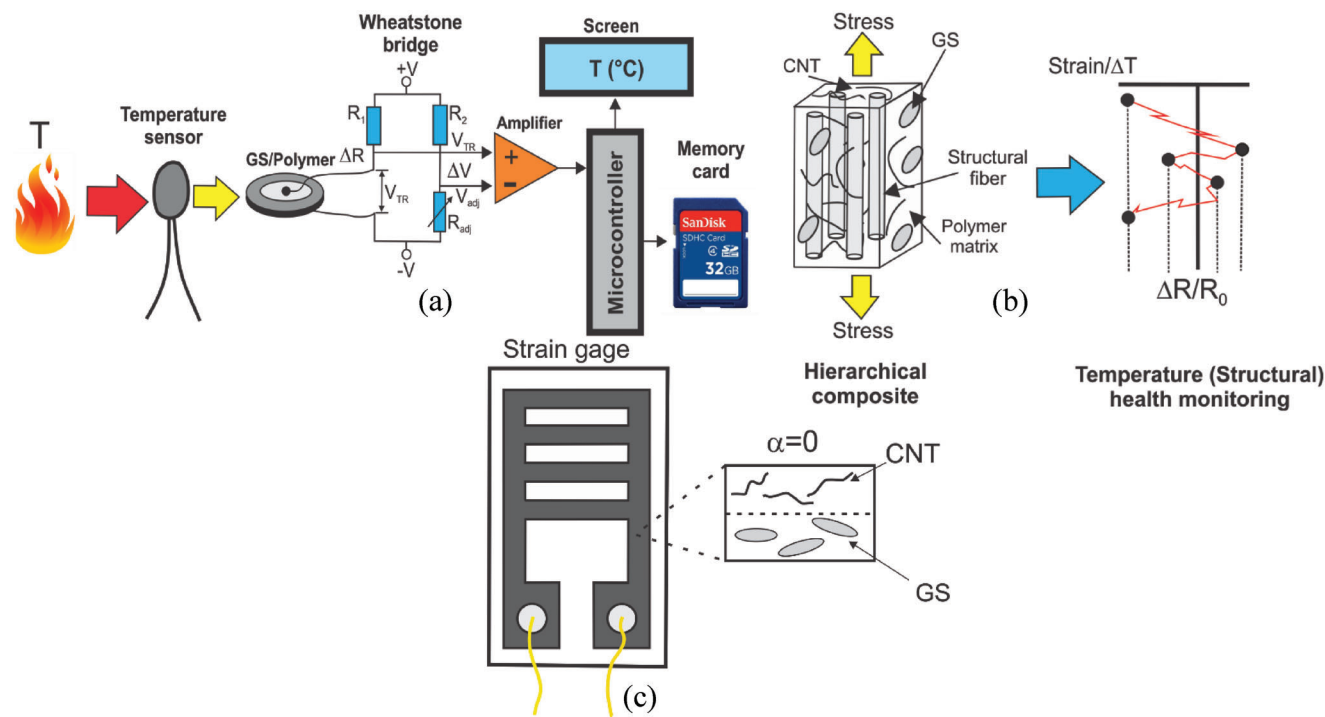


Figure 1. Thermoresistive applications of carbon-based nanostructures and their polymeric nanocomposites. a) Temperature sensors, b) smart structural materials with self-temperature monitoring, c) tailored materials with near-zero temperature coefficient of resistance.

nanotubes and platelets of the family of graphene (collectively referred to as graphenic sheets). Section #4 covers planar carbon-nanostructured arrays (buckypapers) and films. Section #5 covers carbon nanotube fibers and yarns. Section #6 covers the thermoresistive response of polymer nanocomposites filled with carbon nanotubes and graphenic sheets. The discussion focuses on the direct current (DC) electrical response (rather than the alternating current one), since it is the most investigated and most practical modality studied to date. Current issues and an outlook into future directions from the author's perspective is provided in the concluding section (section #7). Published data on thermoresistive coefficients is synthesized for the reader and provided in tabular form within the sections and in an appendix.

2. Fundamentals of Thermoresistivity and its Governing Mechanisms

Thermoresistivity can be defined as the electrical resistance response of a material to changes in temperature ($\Delta T = T - T_0$, where T_0 is the reference temperature, commonly the room temperature). Positive thermoresistivity is defined as an increase in the electrical resistance (R) with increased temperature ($\Delta T > 0$), such as in the case of metals, see **Figure 2**. On the contrary, negative thermoresistivity means that R decreases upon heating, as in the case of semiconductors, see **Figure 2**.

Linear thermoresistivity (which occurs, for example in pure metals over a large temperature range) can be expressed as,^[1]

$$\rho = \rho_0 (1 + \alpha_p \Delta T) \quad (1)$$

where ρ_0 is the electrical resistivity at room temperature and α_p is known as the temperature resistivity coefficient. Copper, for example, has $\rho_0 = 1.67 \times 10^{-6} \text{ } \Omega\text{cm}$ and $\alpha_p = 4.3 \times 10^{-3} \text{ } ^\circ\text{C}^{-1}$.^[1] In pure metals, increased temperature yields atomic lattice scattering, which reduces the electron mobility and decreases the electron mean free path, see **Figure 2** (top).

From an experimental viewpoint, thermoresistivity is commonly expressed in terms of the response curve $R = R(T)$, or by plotting the fractional change of electrical resistance ($\Delta R/R_0$) versus ΔT , where $R_0 = R(T = T_0)$. Substituting R for ρ in Equation (1) and rearranging terms, yields the common equation defining the (linear) temperature coefficient of resistance (α , also known as TCR) such as,

$$\Delta R / R_0 = \alpha \Delta T \quad (2)$$

From a sensors' point of view, the temperature coefficient of resistance (α) is a metric that quantifies the thermoresistive sensitivity.

In semiconductors, upon heating the material, valence electrons gain enough energy to surpass the energy gap and jump to the conduction band, creating more charge carriers. The electrical conductivity of a semiconductor is a function of the concentration of electrons in the conduction band (n), the concentration of holes in the valence band (p), and their corresponding mobilities (μ_n and μ_p), as well as the charge of each carrier (q), such as,^[1]

$$\sigma = nq\mu_n + pq\mu_p \quad (3)$$

For intrinsic semiconductors, at absolute zero temperature all electrons are in the valence band, yielding zero electrical conductivity.^[2] As temperature increases, electrons occupy the energy levels of the conduction band, following quantum mechanics selection rules.^[2] In Equation (3) the number of electrons in the conduction band and holes in the valence band follow an Arrhenius (exponential) equation, where n is exponentially proportional to the temperature. Thus, as T increases the electrical conductivity exponentially increases (the electrical resistivity decreases, see Figure 2).

Semimetals (like graphite) are materials where the valence and conduction bands have a very small overlap. They have a zero band gap and negligible density of states at the Fermi level. They can have positive^[12] or negative^[13] TCs. The semimetallic state is similar to the metallic one, but in the former both electrons and holes contribute to electrical conduction. The physics of semimetals rely on electron-phonon scattering theory.^[12] In these solids, the conduction and valence bands meet at the Fermi level. As a result of their quantum structure, the energy threshold needed for electrons to move from the valence to the conduction band is zero. This yields unique abilities, such as being highly sensitive to magnetic fields and pressure.^[14,15]

Given the strong property-structure relationships described above for carbon-based materials, the response of the electrical resistance to temperature is a fingerprint that physicists and material scientists use to classify solid-state materials.^[1,14,16,17]

For carbon nanostructures such as carbon nanotubes (CNTs), graphene, and multi-layer graphene sheets (GSs) the temperature-dependent electrical response depends strongly

on their number of layers and electronic structure. Charge transport in individual carbon nanostructures is governed by quantum mechanics rules. Singlewall CNTs (SWCNTs) can have a metallic or semiconducting behavior, depending on their structural properties such as their diameter and chirality.^[16,18,19] Multiwall CNTs (MWCNTs) are majorly metallic.^[20,21] This is mostly because of the electronic interactions among the curved graphenic sheets comprising the MWCNT.^[22] It has been argued that the behavior of MWCNTs is metallic, if at least one sheet has a metallic chirality.^[22,23] Other authors^[20,24] have also proposed that only the outer tube contributes to the conductance of MWCNTs. However, mass production of MWCNTs typically yields a combination of metallic and semiconducting ones. On the other hand, graphene (a single-layer) is a zero-gap semiconductor.^[25] As the number of layers increases to two and more, the electronic response becomes that of a semimetal, with band overlapping increasing (toward graphite) with increased number of layers.^[25]

Several quantum mechanics mechanisms have been used to explain the temperature-dependent response of the electrical conductivity of carbon nanostructures, either as individual nanostructures or in the form of arrays or bundles. Among those, the most common mechanisms are variable range hopping (VRH) and fluctuation-induced tunneling (FIT), Figure 2. Both mechanisms predict an exponential decay of the electrical resistivity/resistance as the temperature increases.

The VRH mechanism is a quantum mechanics-based model originally proposed by Mott^[26] for amorphous solids (disorder systems) at very low temperatures, and later extended by Hill.^[27] The VRH model proposes that the thermal energy provided to the material causes electrons to hop from one localized site to another, increasing its electrical conductivity in an exponential fashion. Originally derived for amorphous semiconductors at low temperatures, the model has proved to be successful in explaining the transport behavior of disordered systems and carbon nanostructures.^[26–29] The VRH model predicts a dependence of the electrical conductivity (σ) with the absolute temperature (T) as,^[27,29,30]

$$\sigma = \sigma_0 e^{-\left(\frac{T_M}{T}\right)^\beta} \quad (4)$$

where σ_0 and T_M are constants, and the exponent $\beta = 1/(1+d)$ is related to the dimensionality (d) of the system ($d = 1, 2, \text{ or } 3$). For three-dimensions ($d = 3$), the expression recovers the well-known $T^{-1/4}$ form of the Mott's equation.^[26,27] A linearization of Equation (4) by plotting $\ln(\sigma)$ as a function of $T^{-\beta}$ yields $-T_M^\beta$ as the slope and $\ln(\sigma_0)$ as the intercept with the vertical axis.

For disordered materials characterized by large conducting regions separated by small insulating barriers, Sheng^[31] proposed that the electrical conduction can be ascribed to fluctuation-induced tunneling (FIT). In this mechanism, thermally activated voltage fluctuations across insulating gaps determine the temperature and field dependences of the conductivity. In this model, the probability of electrons tunneling through an insulating barrier increases with temperature, such as,^[29,31,32]

$$\sigma = \sigma_{\text{FIT}} e^{-\left(\frac{T_{\text{FIT}}}{T_{\text{FIT}} + T}\right)} \quad (5)$$

where σ_{FIT} , T_{FIT} , and $T_{1\text{FIT}}$ are constants.

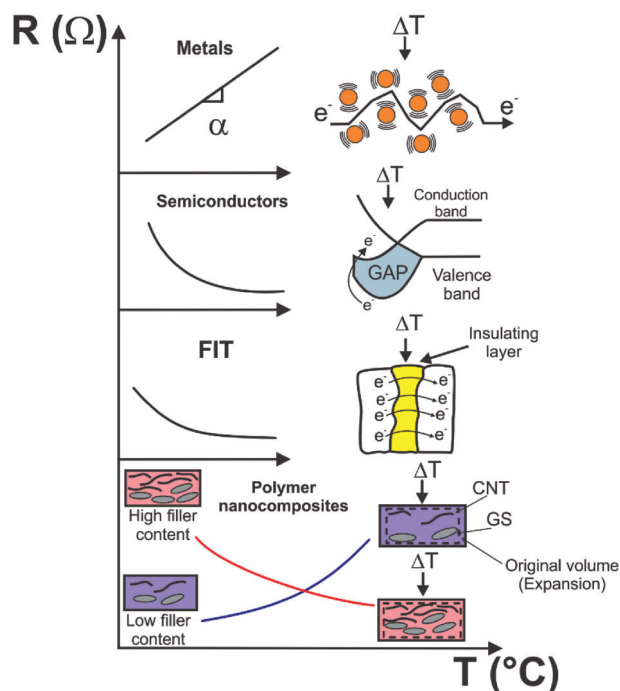


Figure 2. Schematic representation of common thermoresistive mechanisms in solid materials. a) Linear thermoresistivity due to increased electron scattering, b) band theory in semiconductors, c) FIT model, d) polymer nanocomposites with low and high content of carbon nanostructures.

Equation (5) can be linearized by plotting $\ln(\sigma)$ in the vertical axis and $(T_{\text{OFIT}} + T)^{-1}$ in the horizontal axis, yielding $-T_{\text{FIT}}$ as the slope and $\ln(\sigma_{\text{OFIT}})$ as the vertical intercept.

For polymer composites using electrically insulating matrices filled with carbon nanostructures, the situation is markedly different. The electrical conductivity of these composite materials arises from the electro-conductive paths formed by the carbon nanostructures within the polymer. As such, the separation distance between the conductive nanostructures, their contact and tunneling resistances play crucial roles,^[33–38] see Figure 2. Therefore, for these materials, the contribution of the electrical response to temperature of the individual nanostructured fillers may be downplayed by the above-mentioned factors, especially if the filler concentration is low (just above percolation). For polymer nanocomposites with low filler concentration, the positive thermoresistive response commonly observed is governed by the increased separation between nanostructures with increased temperature.^[33,39–43] This is particularly relevant given the high coefficient of thermal expansion and dielectric constant of most host polymers. Upon heating, the separation distance between nanostructures increases, increasing the tunneling resistance. However, for nanocomposites with very high filler concentrations (well above percolation), the individual behavior of the nanostructures and the physico-chemical interactions among them play important roles. For high filler concentrations, the dense network of nanostructures within the polymer contains many redundant pathways. Thus, in the case of high filler content, the contribution of the thermoresistive response of the individual nanostructures and that of the contact resistance among them may become dominant.^[11,44–46] Since those factors may render a negative thermoresistive response, competing mechanisms exist with the thermal expansion of the polymer. For high filler content, these competing mechanisms could even change the thermoresistive response from positive to negative as the filler concentration increases,^[42,47,48] as sketched in Figure 2.

Thermoresistive testing requires measurement of electrical resistance. The vast majority of the works discussed in this review use either a two-point probe or a four-point probe setup. Electrodes are typically cemented by a conductive paint to reduce contact resistance. In a typical four-point probe setup, electrical current is applied at the pair of outer electrodes, while the voltage drop between the inner electrodes is measured. The four-point probe setup is preferred when the contact resistance is of similar order of magnitude than the resistance of the material. This is particularly important for arrays of carbon nanostructures and carbon nanotube yarns, with electrical resistances in the Ω range. For polymeric nanocomposites with electrical resistances in the order of k Ω –M Ω , the two-point probe method may suffice.

3. Thermoresistivity of Individual Carbon Nanotubes and Graphene Sheets

Measuring the electrical response to temperature of individual carbon nanostructures is a very challenging task. One of the most revealing experimental works on electrical and electronic properties of individual carbon nanotubes and their temperature-dependent response is the one by Ebbesen et al.^[3] They conducted dedicated two- and four-point probe electrical resistance measurements of small-diameter MWCNTs at room temperature

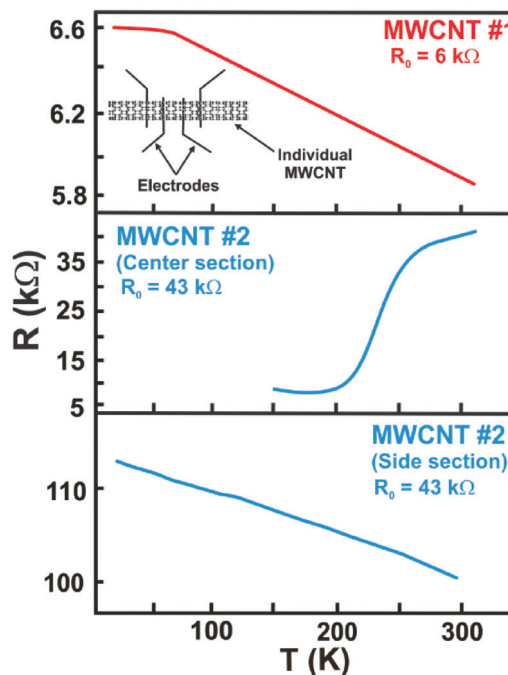


Figure 3. Electrical response to temperature of small-diameter MWCNTs. Adapted from Ebbesen et al.^[3] with permission from Springer Nature.

and in the 4 to 300 K temperature range. Each MWCNT showed a unique conductivity response, i.e., the electrical response was not the same for all MWCNTs measured. Even at room temperature, they found that the MWCNT electrical resistance varied by orders of magnitude. The electrical response to temperature showed various responses. The response of two individual MWCNTs (#1 and #2) selected from the publication of Ebbesen et al.^[3] is shown in Figure 3. The middle and bottom plots correspond to the same MWCNT (MWCNT #2) but measured at different sections. As seen from this figure, both MWCNTs showed very different thermoresistive responses. Even different sections of MWCNT #2 (middle and bottom plots) showed a different electrical response to temperature. MWCNT #1 (top figure) and the lateral section of #2 (bottom figure) showed a fairly linear increase in electrical resistance with decreased temperature, with changes of $\approx 10\%$ for $\Delta T = 296$ K (300 to 4 K). According to Equation (2) and considering that $R_0 = 6.0$ k Ω for MWCNT #1, an estimation of the temperature coefficient of resistance yields $\alpha \approx -3.38 \times 10^{-4} \text{ }^\circ\text{C}^{-1}$, i.e., $-3.38 \times 10^{-2}\%$ per $^\circ\text{C}$. Notice that α is negative because it increases with decreased temperature. Also, given that Equation (2) relies on ΔT (and not on T), the units of ΔT (and hence those of α) can be treated interchangeably as K or $^\circ\text{C}$. Half of the eight MWCNTs tested by Ebbesen et al.^[3] showed a quasi-linear response. However, other MWCNTs showed a sharp decrease in R with decreased temperature, such as the center section of MWCNT #2 in Figure 3.

Even though they presented a negative TCR, Ebbesen et al. argue that these MWCNTs are gapless metallic materials, and that the temperature dependence comes from another mechanisms, such as changes in the carrier concentration and mobilities.^[3] Other authors have also proposed that the electron-phonon scattering mechanisms that govern the TCR of SWCNTs and

MWCNTs depend on the nanotube length.^[49] Given their dimensions, the electrical response to temperature of individual CNTs have undoubtedly a quantum nature. Langer et al.^[50] found a logarithmic dependence of the electrical conductance with temperature for individual MWCNTs. They explained such behavior in terms of two-dimensional weak localization and universal conductance fluctuations in mesoscopic conductors. They concluded that the electrical transport in MWCNTs is governed by electron interference effects occurring in disordered conductors with a reduced dimensionality. Kane et al.^[51] proposed that the quasi-linear electrical response to temperature of armchair metallic SWCNTs can be explained by quantum mechanics coupling of the conduction electrons to long-wavelength torsional shape fluctuations. However, although their theory may be valid for individual CNTs, their measurements were conducted for CNTs in the form of ropes or mats (randomly oriented entangled ropes). To date, it is known that the electrical response of individual CNTs may significantly differ from that of bundles of CNTs, i.e., arrays, mats, buckypaper, fibers, yarns. This is mostly because of the contact and tunneling resistances among the CNTs, and the quantum phenomena which occur among the CNTs when acting as a physico-chemically interacting group. In fact, Skákalová et al.^[52] tested individual CNTs (SWCNTs and MWCNTs) and networks of them with various thicknesses. They found that the temperature dependence of the electrical conductivity depends on the thickness of the CNT network, and can be explained by hopping conduction and tunneling through thin barriers separating metallic regions. Further discussion concerning the electrical response to temperature of groups (arrays) of carbon nanotubes will be presented in section 4.

Graphene (a single-layer) is a zero-gap semiconductor with linear energy-momentum dispersion around the Fermi energy.^[25] However, as the number of layers increases toward “few-layer graphene”, the valence and conduction bands overlap, becoming a semimetal.^[25,53] That is, the electronic behavior of multilayer graphenic materials approximates that of graphite (a semimetal) as the number of layer increases. Using tight-binding calculations, Partoens and Peeters^[25] found that for more than 10 layers, the difference in band overlap with bulk graphite (41 meV) is less than 10%. Therefore, the electrical response to temperature of few-layer and multilayer graphene strongly depends on the number of layers.

Shao et al.^[54] report thermoresistive tests of single-layer and bilayer graphene materials obtained from mechanical exfoliation of highly oriented pyrolytic graphite. The graphene films were supported by a thicker insulating oxide layer and two Pt electrodes were added for thermoresistive characterization. Characteristic Raman fingerprints proved the single-layer and bilayer character of the graphene materials. They heated the graphene materials from room temperature ($T_0 = 300$ K) to 500 K and found a negative dependence of the electrical resistance to temperature, as shown in **Figure 4**. When heated from 300 to 500 K, the electrical resistance of single-layer graphene decreases about 30% ($R/R_0 \approx 0.7$). A linear fit to the data plotted by Shao et al.^[54] yields $\alpha \approx -0.15\%$ per °C, according to Equation (2). For the bilayer material, on the other hand, the decrease at 500 K is about 70% ($R/R_0 \approx 0.3$), i.e., a significantly higher thermoresistive sensitivity. For this case, a linear fit to the published data yields $\alpha \approx -0.35\%$ per °C. This is one order of magnitude higher than the one reported

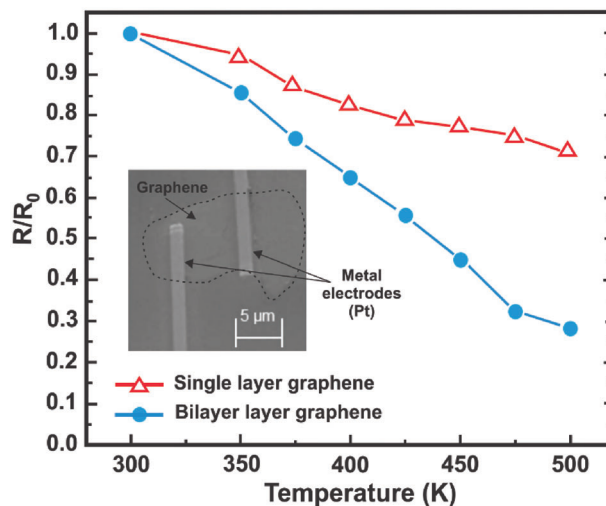


Figure 4. Electrical response to temperature of single-layer and bilayer graphene. Reproduced from Shao et al.^[54] with permission from AIP Publishing.

by Ebbesen et al.^[3] for MWCNTs (see Figure 3). The thermoresistive behavior of these graphene-based materials was explained by a quantum mechanics model on the basis of thermal generation of carriers and electron/hole scattering with acoustic phonons.^[54] One thing to bear in mind is that in this, as in most experiments characterizing the electrical properties of single-layer graphene, the graphene layer is not free-standing but supported by a thicker (electrically insulating) substrate. This could play thermal and/or mechanically constraining roles, see, e.g., ref. [55].

For few-layer graphene (3-4 layers) grown on electrically insulating ceramic substrates, Huang et al.^[56] found a TCR of $-3.52 \times 10^{-2}\%$ per °C. Several other works have also reported a negative TCR for graphene and its few-layer derivatives.^[6,10,57-59]

Depending on the application, a high or negligible TCR can be sought for materials based on graphene and its few-layer derivatives. On the one hand, very high TCRs are sought in applications such as temperature sensors and bolometers, i.e., devices used for measuring radiant heat.^[6,60-62] On the other hand, zero or negligible TCRs are sought in sensing applications when the transduced variable is different to temperature, but also causes changes in electrical resistance. In those cases, the variation of electrical resistance with temperature is deemed a spurious effect. For example, for strain sensing devices that work with the piezoresistive phenomenon,^[7,63-65] changes in electrical resistance produced by temperature are an undesired effect that needs to be compensated. Therefore, in such applications, temperature-independent sensors comprising a material or combination of materials with zero TCR are sought. The negative TCR of graphene has been exploited for such an aim, by combining graphene or few-layer graphene with other materials with positive TCR such as platinum, palladium, gold, graphene oxide, or carbon hybrids.^[4,10,58,65,66]

The electrical response to temperature of graphene and its few-layer derivatives can be affected by the synthesis method, thickness, lateral size, amount, and type of functional groups, among others. Davaji et al.^[55] reported positive TCRs in a small temperature range (10 to 30 °C) for free-standing graphene and graphene

over SiO₂/Si substrates growth by chemical vapor deposition. Boon et al.^[67] reported that reduced edge-oxidized graphene oxide (by using nitric acid) can change from positive to negative TCR by introducing structural defects in its basal plane. Thus, not only material combinations, but also functionalization may be used to tailor the temperature dependence of the electrical resistivity of graphene-based materials.

4. Thermoresistivity of Carbon Nanotube and Multilayer Graphene Arrays and Films

Since individual CNTs and single-layer graphene are very difficult to handle, the vast majority of publications dealing with the science and engineering of carbon nanomaterials have used some form of multi-layer graphene films, entangled arrays, bundles, or buckypapers, either free-standing, deposited over a thicker substrate or as an integral part of a multi-layered material.^[63,66,68–74] The mechanisms governing thermoresistivity in these entangled materials may differ significantly from those of individual CNTs or graphene. This is because in these arrays electrical charge flow occurs through a network, and not only within individual carbon nanostructures. Thus, the mean free path changes and electrical conduction is no longer confined to quantum (through-thickness) or micro-size (lateral dimensions for graphene or CNT length) paths. Collective (interacting) mechanisms arise, which may yield nonlinearities and trigger new phenomena not observed for individual nanostructures, see, e.g., ref. [52,69,75]. For example, Skákalová et al.^[52] conducted electrical measurements of SWCNT buckypapers ($\approx 35 \mu\text{m}$) and SWCNT networks of different thickness on a SiO₂ substrate, characterized by an optical transparency ranging from 30% to 90%. They found that the temperature response of the electrical conductivity depends on the network thickness (i.e., transparency). They argue that the electrical response of the thinner networks is consistent with hopping conduction, while that of the thickest ones obeys tunneling through thin barriers separating metallic regions.

The mechanisms governing the thermoresistivity of carbon-nanostructured arrays may be viewed as analogous to those of piezoresistivity.^[76] However, in the case of thermoresistivity, the mechanisms are driven by temperature, instead of strain. As a general classification, it is proposed here that the thermoresistive mechanisms occurring in arrays of carbon nanostructures can be broadly classified into three groups of mechanisms, as schematically depicted in **Figure 5** for graphenic sheets (GS, left) and CNTs (right). The generic term “graphenic sheets” is used herein to broadly encompass the single-, few-, and multilayer-graphene derivatives.

The first mechanism (indicated by a straight double-ended arrow) is the inherent electrical response of the individual carbon nanostructure to temperature. This comprises classical electrodynamics and quantum electroconduction phenomena at the graphene (or CNT) level.^[3,24,53] The second and third mechanisms refer to collective (group) phenomena triggered by particle-to-particle physico-chemical interactions upon heating or cooling. If there is physical contact or overlapping between nanostructures, a contact resistance develops, which is depicted in Figure 5 by a small (blue) resistor. The particle-to-particle contact resistance is a function of temperature, and also of the geometry of the contacting particles, contact area, free charge carrier

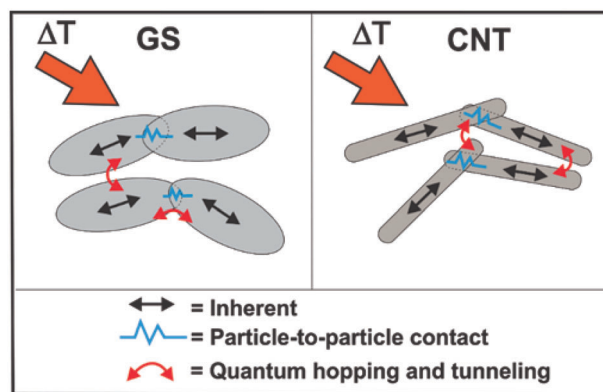


Figure 5. Thermoresistive mechanisms occurring in groups (arrays) of carbon nanostructures.

concentration, and density of functional groups, among others, see, e.g., ref. [77,78]. Finally, the (red) bent double-ended arrows represent non-contact interactions among groups of nanostructures. Assisted by temperature, free electrons of the conductive nanostructures separated by a nanometric thin electrically insulating layer may hop or tunnel.^[26,31,52,79] The tunnel current is expected to vary exponentially with the thickness of the insulating layer,^[80] i.e., air in the case of porous arrays of carbon nanostructures. Although the maximum distance that electrons in these conditions could quantumly tunnel is yet uncertain, tunneling distances up to a few nanometers are commonly accepted and used in computational models.^[79–82] Other quantum phenomena assisted by temperature such as variable range hopping and fluctuation-induced tunneling (see section 2) also fall into this third category, and are expected to strongly influence the thermoresistive response of carbon-nanostructured arrays.^[26,27,31] All three thermoresistive mechanisms simultaneously coexist for arrays, films, buckypapers or groups of carbon nanostructures. The relative contribution of each one varies depending on factors inherent to the nanostructures themselves (size, functional groups, etc.) and on factors related to the dispersion, distribution, orientation and concentration of the network of nanostructures. For dense arrays, buckypapers, films or carbon nanostructures deposited over thicker substrates, the collective mechanisms may dominate over the inherent response of the individual nanostructures. Evidence of these can be inferred from the distinctive change in thermoresistive response of individual nanostructures compared to that of networks comprising thousands of the same carbon nanostructures, see, e.g., Skákalová et al.^[52]

Given the above-mentioned factors, the thermoresistive response of carbon-nanostructured arrays and films presents large variability, reporting positive and negative TCRs. A summary of published TCRs for carbon nanotube arrays (bundles, buckypapers, etc.) and films is listed in **Table 1**. All TCRs (α) listed in the Table 1 and in the subsequent tables are reported in units of $\%^\circ\text{C}^{-1}$, i.e., 10^{-2} per $^\circ\text{C}$. In this regard, published data in K^{-1} were simply transcribed as $^\circ\text{C}^{-1}$, without adding or subtracting any quantity related to unit conversion. This is because α operates over a difference in temperature (ΔT), and ΔT remains the same regardless of whether the Kelvin or Celsius scale is used. Unless indicated with a letter “c”, the actual TCR number was

Table 1. Temperature coefficient of resistance of carbon nanotube arrays and films.

Description	Temperature Interval [°C]	α [% per °C]	Ref.
Thymine functionalized MWCNT bundles over silicon	25 to 35	-5.6 (nl)	[62]
MWCNT-coated PDMS	N/A	-0.52	[83]
MWCNT array on PET film	-40 to 100	-0.4	[84]
MWCNT bundles on paper	25 to 100	-0.31 to -0.49	[85]
MWCNT array assembled on paper	20 to 75	-0.27 (c, nl)	[68]
MWCNT bundles	25 to 80	-0.125 to -0.155	[92]
MWCNT film	-5 to 45	-0.1	[93]
MWCNT bundles on PET	25 to 50	-8.92×10^{-2}	[94]
MWCNT bundles between silver	26 to 67	-8.81×10^{-2}	[95]
MWCNT film	-63 to 17	-8×10^{-2}	[89]
Aligned MWCNT arrays over glass	25 to 160	-8×10^{-2}	[88]
MWCNT buckypaper	30 to 120	-7.53×10^{-2}	[96]
MWCNT buckypaper within a glass/epoxy composite	25 to 150	-7.18×10^{-2}	[72]
Free-standing MWCNT film	-270 to 147	-7×10^{-2}	[97]
MWCNT vertical arrays	35 to 125	-4.73×10^{-2}	[98]
MWCNT array	25 to 190	-4.62×10^{-2}	[99]
MWCNT array	0 to 100	-3.6×10^{-2} to -0.27	[91]
MWCNT assembly	≈ 25	0.3	[70]
MWCNT array	≈ 25	0.27	[86]
MWCNT films	30 to 400	2.8×10^{-2}	[87]
SWCNT vertical assembly	65 to 25	-0.16 to -0.78	[69]
SWCNT film	-63 to 17	-0.17	[89]
SWCNT buckypaper	-270 to -153	Negative	[90]
SWCNT array	0 to 100	0.539 to 0.849	[91]

(c): Calculated (estimated) from published plot or numerical data. (nl): Curve is non-linear, a linear estimate was carried out. PET: polyethylene terephthalate. PDMS: Polydimethylsiloxane. N/A: Not available.

published in the original reference. In a few cases where only a curve or numerical data is provided, a linear estimation was conducted, and such an estimation is indicated in the table with the letter “c” (for “calculated”). Reading numerical data points from reported plots was electronically conducted aided by the free online software “Plot Digitizer” (pOrbital, 2023). A few curves are also nonlinear, and this is indicated in the table with the letters “nl”. In such nonlinear cases, curve fitting was conducted using the first and last data points of the curve. For MWCNT arrays the large majority of the published TCR data is negative, and the large majority of the data reported in Table 1 ranges from -0.04 to -0.15 . A few outliers are observed with higher (negative) absolute values.^[62,68,83–85] These works with significantly higher neg-

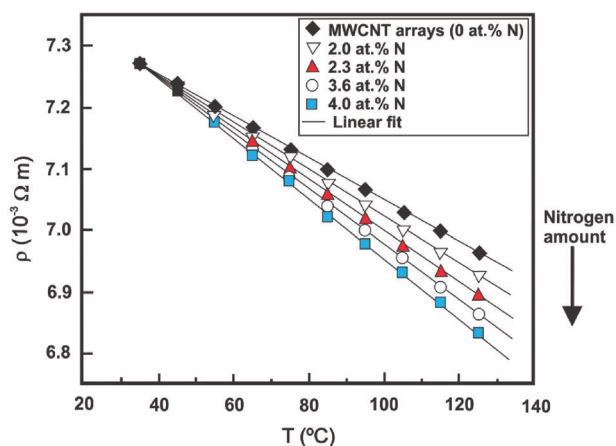


Figure 6. Effect of nitrogen concentration on TCR of MWCNT films. Reproduced from Ionescu et al.^[98] with permission from Elsevier.

ative value of TCR have in common that the MWCNTs are not free-standing but deposited over a substrate (mostly polymeric), which is expected to play a role. A few works have also reported positive TCRs for MWCNT arrays,^[70,86,87] see Table 1. As a reference, Platinum, which is commonly used for commercial thermistors, has a (positive) TCR of 0.393% per °C.^[88] Arrays of SWCNTs have also reported negative^[69,89,90] and positive^[91] TCRs, of magnitudes that fall within the range of those reported for MWCNT arrays.

The variability observed in the TCRs listed in Table 1 is because the electrical response to temperature of carbon-nanostructured arrays depends on several factors, such as the length and physical properties of the CNTs, their packing density (porosity), CNT functionalization, and if they are truly free-standing or supported by a substrate. Even when the substrate is electrically insulating, the thermomechanical properties of the substrate can play a role, especially for polymers with a high coefficient of thermal expansion.

The synthesis conditions can also affect the TCR. Using spray pyrolysis chemical vapor deposition, Ionescu et al.^[98] grew vertically aligned MWCNTs using xylene as the carbon feedstock and acetonitrile as the nitrogen feedstock. They found that the amount of nitrogen incorporation significantly influences the growth rate, morphology and structure of the nanotubes, and consequently their electrical response to temperature, see Figure 6. The TCR was $-4.72 \times 10^{-2}\%$ per °C for MWCNT films produced using only xylene, decreased 22% ($-5.78 \times 10^{-2}\%$ per °C) for MWCNT films obtained from 50 vol.% xylene:acetonitrile (2.3 at.% N in Figure 6), and further decreased to -6.69% per °C (42%) for the MWCNT films synthesized using pure acetonitrile (4.0 at.% N in Figure 6).

Functionalization is also a factor that affects the electrical response to temperature of carbon nanostructures. Kumar et al.^[95] found an increase in TCR from -8.81×10^{-2} to -0.13% per °C when MWCNT arrays were functionalized with nitrogen. They hypothesize that the higher TCR may be due to the creation of donor states by the nitrogen functionalization, which yields higher electron density near the Fermi level.

Numerically similar negative values of TCRs have been reported for films or buckypapers made of few-layer or multilayer

Table 2. Temperature coefficient of resistance of graphenic films.

Description	Temperature Interval [°C]	α [% per °C]	Ref.
RGO film on SiO ₂	10 to 40	-0.95 to -0.68	[100]
GS layer over alumina	0 to 100	-0.52	[74]
RGO layer over Kapton	-43 to 100	-0.209	[65]
GS buckypaper over a dielectric layer	-60 to 60	-0.155	[73]
Few layer graphene film on ceramic	25 to 350	-3.52×10^{-2}	[56]
Graphene/RGO film	-70 to 120	-3.25×10^{-2}	[4]
RGO film	-263 to 2726	Negative (nl)	[61]
Graphene films on SiO ₂	25 to 200	0.168 to 0.27	[5]
GS ink (in acrylic polymer) on a plastic substrate	-5 to 57	0.15	[71]
Graphite film over paper	40 to 100	0.12 (c,nl)	[66]

(c): Calculated (estimated) from published plot or numerical data. (nl): Curve is non-linear, a linear estimate was carried out. RGO: Reduced (few or multilayer) graphene oxide.

graphene and reduced graphene oxide (RGO), as observed from Table 2. As seen from this table, positive values are far less common than negative ones. Notice that the last three rows in Table 2 report positive TCRs, and they have in common being deposited over a substrate.

For graphene, the size of the graphene sheet could also play a role in its electrical response to temperature. Debroy et al.^[5] reported that the TCR of graphene interconnections on SiO₂/Si substrates decrease with decreasing the ribbon's width. A 38% decrease in TCR was reported when decreasing the graphene width from 1 μm to 300 nm.

Another field of interest for graphenic materials is the development of zero-TCR materials. Zero-TCR materials are of great interest for the development of temperature-independent sensors, such as strain or moisture sensors. By using a hybrid combination of graphene, carbon nanotubes or graphenic arrays with negative TCR and another material such as metallic or graphite particles with positive TCR, zero TCR can be targeted.^[4,10,11,58,101] For example, Nuthalapati et al.^[65] found that by tuning the multilayer RGO:Paladium ratio the TCR can be tuned from negative (RGO) to positive. Amjadi and Sitti,^[66] Figure 7, proposed a hybrid combination of graphite microparticles (positive TCR) and CNTs (negative TCR) to produce hybrid films with nearly zero TCR. The film named "Hybrid 1" had a CNT-to-graphite mass ratio of 0.08, hybrid 2 of 0.10, and hybrid 3 of 0.12. In Figure 7, it is seen that the positive TCR of graphite can be tuned by the introduction of CNTs, forming hybrid films (hybrids 1 to 3) with near zero TCR.

5. Thermoresistivity of Carbon Nanotube Fibers and Yarns

Carbon nanotube fibers either in the form of aligned networks or twisted yarns are extraordinary hierarchical materials that aim to translate the superior properties of carbon nanotubes to macroscopic structural fibers, see, e.g., ref. [102,103]. CNT aligned fibers and CNT yarns (CNTYs) are hierarchical structures comprising CNTs as building blocks at the fundamental (nanomet-

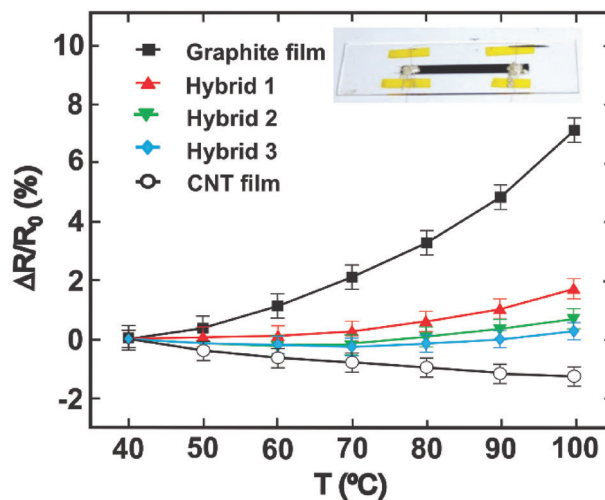


Figure 7. Electrical response to temperature of graphite, CNT and graphite-CNT hybrid films. Reproduced from Amjadi and Sitti.^[66]

ric) level, bundles of CNTs held together by friction, twist (in the case of yarns) and van der Waals forces at the microscopic level, and thicker fibrils (made of thinner bundles) at the mesoscopic level. They are continuously long fibers with extraordinary electrical conductivity and toughness, which can be exploited for the development of smart structural materials.^[104,105] Understanding their thermoresistive response may be more challenging than for individual carbon nanotubes or conventional carbon fibers, given their hierarchical structure and collaborative response. Conventional pitch-based carbon fibers typically present a negative TCR, which is attributed to the increase in the density of electrical charge carriers with increased temperature.^[106] The situation, however, is more complex for CNT fibers and twisted yarns, given their high porosity and very strong structure-property relationship. The density of CNT-to-CNT and bundle-to-bundle contacts and the spacing among them (for hopping or tunneling) strongly influences the electrical response of such fibers, and thus is expected to govern their thermoresistive response. Lekawa-Raus et al.^[107] proved that the synthesis conditions strongly affect the thermoresistive response of CNT fibers, showing a strong structural-electrical dependence. Using CNT fibers spun from a floating catalyst process, they reported thermoresistive responses which are strongly nonlinear, nonmonotonic, and negative for the large majority of the temperature range investigated. Niven et al.^[108] also found nonlinear negative thermoresistive responses for dry-spun MWCNT yarns. They annealed the CNTYs up to 2700 °C in argon and showed that the thermoresistive response and hysteresis under heating-cooling cycles can be affected by the annealing temperature and presence of adsorbed species.

The most accepted mechanisms governing the thermoresistive response of CNT fibers and yarns are the VRH and FIT ones, described in Section 2 and represented by Equations (4) and (5). Zhang et al.^[29] investigated the electrical response to temperature of direct spun CNT fibers from 25 to 1100 °C in nitrogen atmosphere. The authors observed a nonmonotonic thermoresistive response, which they classified into two zones (I and II in Figure 8). From 25 to 250 °C (zone I, $T_c \approx 250$ °C) the behavior

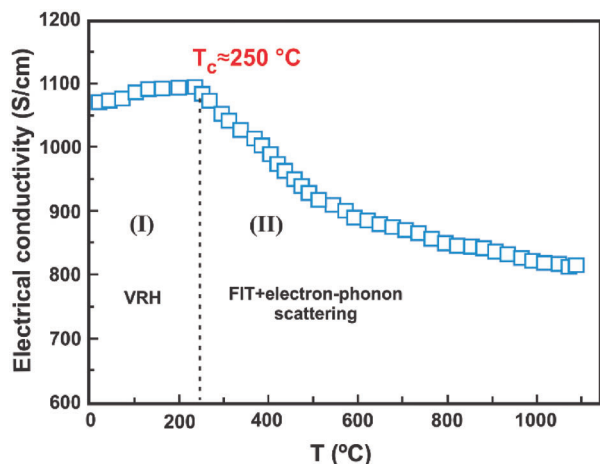


Figure 8. Electrical conductivity as a function of temperature for direct-spun CNT fibers. Reproduced from Zhang et al.^[29] with permission from AIP Publishing.

was explained by the VRH model, Equation (4), consistent with a three-dimensional hopping mechanism.

Curve fitting of the experimental data within this range to Equation (4) yielded $\sigma_0 = 1370 \text{ S cm}^{-1}$, $T_M = 1.2 \text{ K}$ and $\beta = 1/4$. The authors suggest that the $\beta = 1/4$ exponent correlates with three-dimensional hopping among defective CNTs and their bundles. Above $T_c = 250 \text{ }^\circ\text{C}$ (zone II in Figure 8) the experimental data fits well to what they called a “heterogeneous model”, which is the sum of the FIT model of Equation (5) and an exponential term due to electron-phonon scattering.

Other authors have also used either the VRH^[30,109,110] or the FIT^[110] models to describe the thermoresistive response of CNT fibers and twisted yarns.

For CNT fibers and yarns, it is not rare that within a given temperature interval the experimental data can be approximated as linear, so a TCR can be calculated. A summary of TCRs reported in the literature for CNTYs is shown in Table 3.

From Table 3, it is seen that the collected data evidence a negative thermoresistive response for CNTYs, with TCRs ranging approximately from -0.12 to -0.06% per $^\circ\text{C}$. Notice that most of the data in Table 3 are close to -0.1% per $^\circ\text{C}$, which may be taken as a quick reference value. This number falls within the range of the TCRs reported in Table 1 for CNT arrays, but the absolute

Table 3. Temperature coefficient of resistance of CNTYs.

Temperature Interval [$^\circ\text{C}$]	α [% per $^\circ\text{C}$]	Ref.
20 to 75	0.12	[111]
196 to 25	0.1	[102]
25 to 30	9.54×10^{-2}	[110]
25 to 100	9.46×10^{-2}	[110]
≈ 22	0.075 TO 0.13	[112]
25 to 80	7.5×10^{-2}	[113]
256 to 27	6.8×10^{-2}	[109]
30 to 103	5.7×10^{-2} (c)	[114]

(c): Calculated (estimated) from published plot or numerical data.

value is a bit smaller than some of the negative data in such a table. This may be due to the increased number of contact points in continuous and twisted CNTYs. Comparison with individual CNTs is more challenging, given the strong structure-property relationships of these materials. As pointed out in section 3, for individual MWCNTs growth by carbon-arc and annealed in argon, Ebbesen et al.^[3] reported TCRs of $\approx -3.38 \times 10^{-2}\%$ per $^\circ\text{C}$, which is smaller than those reported in Table 3 for CNTYs. However, a fair comparison would require the use of the same individual CNTs comprising the yarn, and reports of such kind of hierarchical experiments are not found in the literature.

Balam et al.^[110] reported cyclic heating-cooling thermoresistive tests of individual dry-spun CNTYs in two regimes, above (from 25 to $100 \text{ }^\circ\text{C}$, Figure 9a) and below (from 25 to $-30 \text{ }^\circ\text{C}$, Figure 9b) room temperature.

They found similar (negative) TCRs in both regimes, above ($-9.46 \times 10^{-2}\%$ per $^\circ\text{C}$) and below ($-9.54 \times 10^{-2}\%$ per $^\circ\text{C}$) room temperature, supported by the VRH and FIT mechanisms. The hysteresis loop between the heating and cooling curves was significantly lower for experiments below room temperature, as seen in Figure 9a,b. The hysteresis also greatly increased when the individual CNTY was embedded into a thermosetting polymer.

Given the high porosity of the yarns, the electrical response of CNTYs is sensitive to the ingress of fluids and polymeric resins. This can be exploited to develop resin flow sensors and sensors that assist in online monitoring of the curing kinetics of thermosetting resins.^[115,116]

6. Polymer Nanocomposites Filled with Carbon Nanotubes and Graphenic Sheets

Polymer nanocomposites filled with carbon nanostructures share with arrays of carbon nanostructures (films or buckypapers) the thermoresistive mechanisms described in Section 4 (Figure 5). However, these materials exhibit unique mechanisms that are absent in arrays, which stem from the host polymer matrix. Two major contributions that arise from the polymer matrix are the thermal expansion/contraction of the polymer and the modification of the tunneling and hopping electrical resistances.^[35–37,117] The simulations of Gong et al.^[36] propose three major mechanisms governing the thermoresistivity of CNT polymer composites, viz., thermal expansion of the matrix, thermally assisted tunneling, and thermally activated hopping. These mechanisms have also been recognized by other authors, supported by simulations and experiments.^[37,42,117,118] In this case, the tunneling barrier existent between arrays of carbon nanostructures is no longer filled with air, but with a dielectric polymer. This modifies the dielectric permittivity of the insulating medium and hence modifies the value of the height of the tunneling barrier. Since the tunneling resistance depends exponentially on the square root of the tunneling barrier height,^[37,82] this significantly modifies the tunneling electrical resistances and their response to temperature.^[35,118]

The coefficient of thermal expansion of the polymer plays a paramount role in the thermoresistive response of carbon-nanostructured polymer composites upon heating/cooling. The relative contribution of the thermal expansion/contraction of the polymer to the global thermoresistive response is particularly

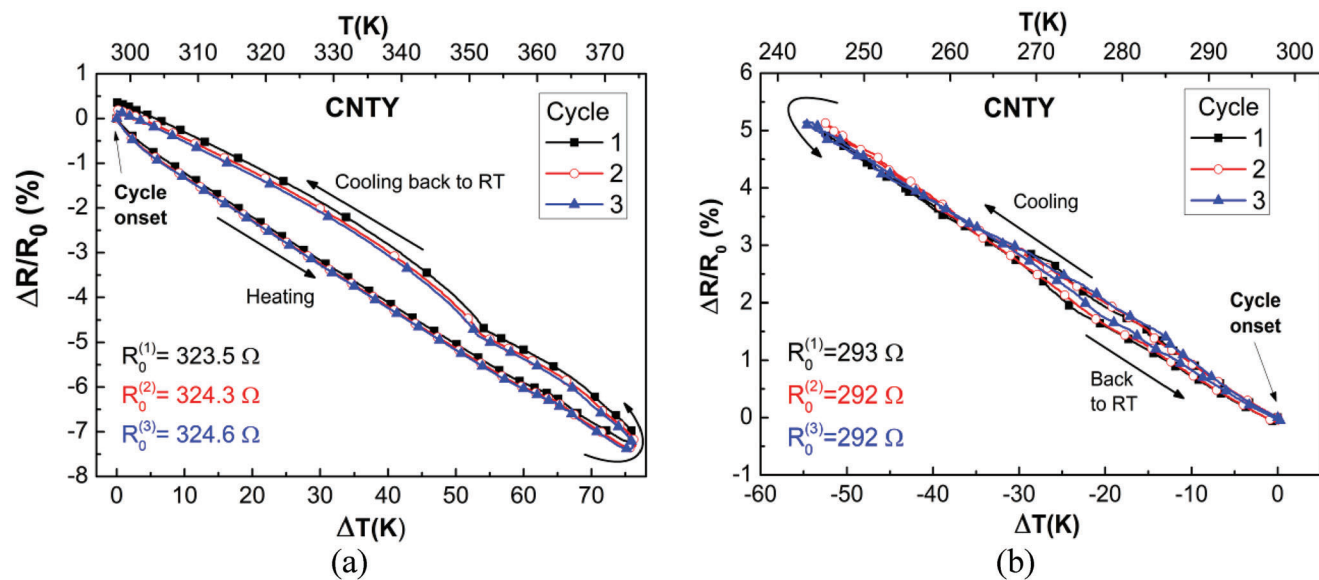


Figure 9. Thermoresistive response of individual CNTYs tested in two temperature intervals. a) Above room temperature, b) below room temperature. Reproduced from Balam et al.^[110] with permission from John Wiley & Sons.

important for carbon-nanostructured polymer composites with low filler content.^[37,42,117] The glass transition temperature of the polymer must be also taken into account. Gong et al.^[36] argue that above the glass transition temperature of the polymer, the transport mechanism experiences a transition from tunneling to hopping, which increases the thermoresistive sensitivity. However, one must bear in mind that thermoresistivity must be reversible, and above the glass transition temperature its practical application may be compromised by irreversibility and hysteresis.

Higher TCRs are typically achieved at lower carbon nanofiller concentrations, i.e., for sparser GS or CNT networks just above the electrical percolation threshold.^[35,42,119] In fact, Cen-Puc et al.^[42] reported that for MWCNT/polysulfone films, the electrical response to temperature switches from positive TCR at low filler concentrations (0.5 to 10 wt%) to negative TCR at high filler concentrations (≥ 40 wt%), **Figure 10**. Near-zero TCRs can be achieved by tuning the nanostructured carbon filler concentration, as shown by the 25 wt% curve in Figure 10. In this case, the higher (positive) TCRs obtained for the composites with lower MWCNT concentrations are attributed to the dominance of the thermal expansion of the matrix, which drives the MWCNTs apart upon heating.

This trend, from positive TCR at low MWCNT concentrations to negative TCR at higher filler concentrations, has also been experimentally observed by other authors using a different polymer matrix,^[120] as well as predicted by Monte Carlo simulations.^[117] Gao et al.^[121] reported that thermally treating SWCNT/polyimide films is another possible way to tune their TCR.

Table A1 in Appendix A summarizes TCRs collected for polymer composites filled with either carbon nanotubes or graphenic sheets (GSs). The majority of the TCR values reported in Table A1 were directly reported as numerical data in the original publications. Reading numerical data points from reported plots was electronically conducted aided by the free online software “Plot

Digitizer” (pOrbital, 2023). For those publications where the actual TCR was not directly reported, and the available data made it possible, the TCR was estimated through linear curve fittings in the temperature intervals reported in the table. Nonlinear thermoresistive ($\Delta R/R_0$ vs ΔT) response curves are not rare, and in such cases the definition of the TCR through Equation (2) is compromised. For such cases, the TCR may be reported as a function of temperature,^[9,119] by approximating one or various linear fittings within selected temperature intervals,^[110] or simply by reporting the full thermoresistive response curves.^[33,40,122–124]

There is significantly more data published on CNT/polymer composites than on GS/polymer ones. For GS/polymer composites, the morphology (lateral size, number of layers) and

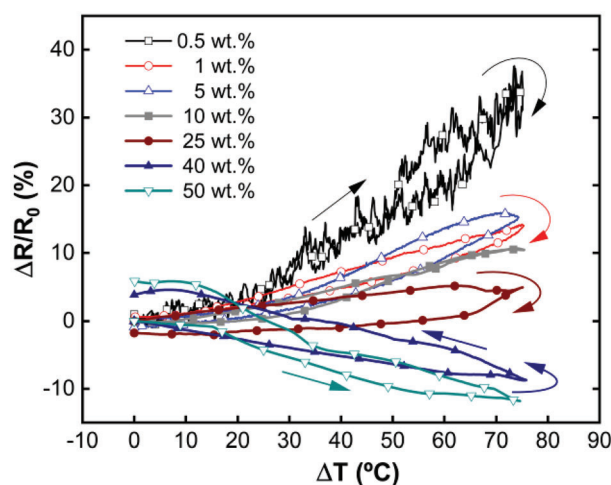


Figure 10. Thermoresistive response of MWCNT/polysulfone composites at different MWCNT concentrations. Reproduced from Cen-Puc et al.^[42] with permission from Elsevier.

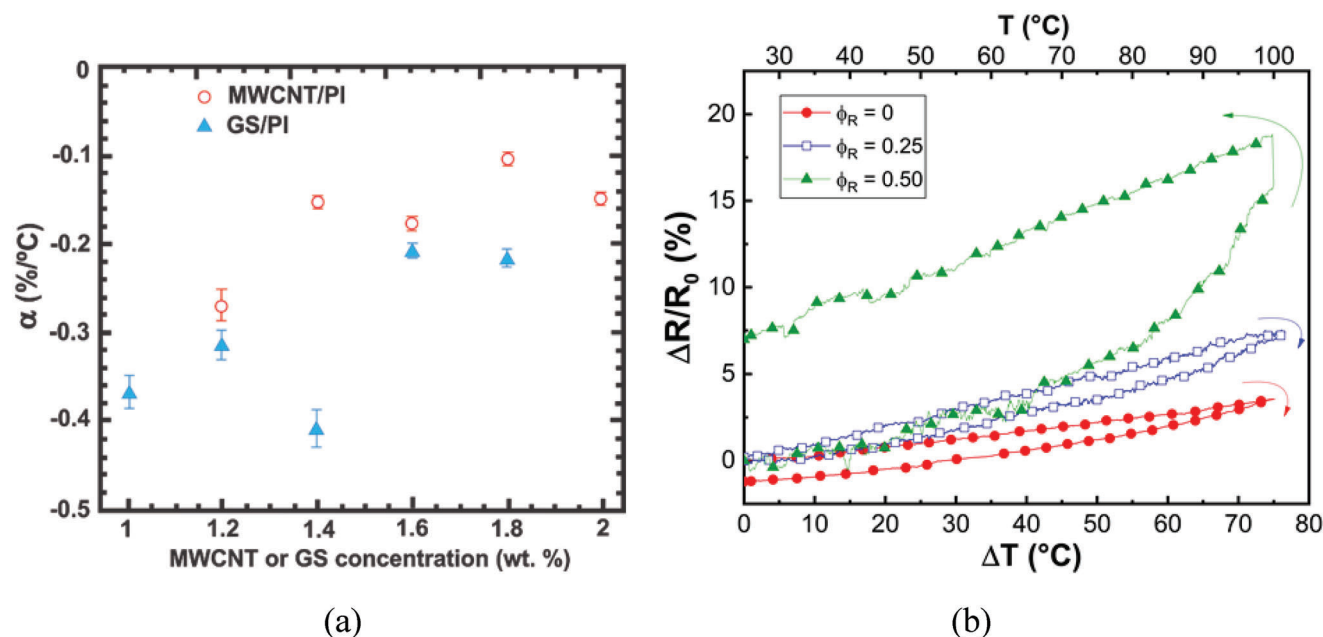


Figure 11. Influence of filler type (a), reproduced from Li et al.^[46] with permission from Elsevier, and hybrid filler relative concentration (b), reproduced from Pech-Pisté et al.^[43] with permission from Elsevier, on the thermoresistive response of carbon-nanostructured polymer composites.

physicochemical properties (surface area, functional groups) of the graphenic sheets is of paramount importance for the formation of the electroconductive network, see, e.g., ref. [125]. However, the physicochemical properties of the GSs are rarely provided in publications reporting the thermoresistive response of polymer composites, so reliable structure-property relationships which drive fundamental conclusions are hard to construct.

Both, negative (e.g., ref. [46,122,126–130]) and positive (e.g., ref. [9,33,34,123,131,132]) TCRs have been reported, as evidenced in Table A1. The sign of the TCR (positive or negative) depends on many factors, such as the filler type and their physicochemical properties, the thermo-mechanical properties of the polymer matrix, and the temperature interval. As for the magnitude, most of the data collected in Table A1 is on the order of 10^{-1} % per °C (either positive or negative) and all data falls between -9.76 % per °C and 6.74 % per °C. With the current information available, it is unclear if GSs or CNTs may provide enhanced thermoresistive sensitivity. The current scientific evidence suggests that factors such as the in-plane dimensions (lateral size) of the GS (or length in the case of CNTs), their physicochemical properties, and their state of functionalization may be more relevant than the actual filler type (GS vs CNT). In any case, for polymer composites at relatively low filler concentrations, the thermomechanical properties of the matrix and the state of dispersion of the filler within the matrix may be more relevant than the intrinsic thermoresistivity of the filler. More systematic investigations are needed to shed light on this issue. As an example, Li et al.^[46] compared the TCRs of films made of a polyimide matrix and either MWCNTs or GSs. According to their findings (Figure 11a), the absolute value of the TCR was slightly higher for nanocomposites using GSs as fillers. However, no information on the structural and physicochemical properties of the carbon fillers used was provided in such a

publication, so the actual reasons for this difference are hard to assess.

An alternative that has been recently explored is the use of hybrid carbon-nanostructured networks of different dimensionality.^[43,133] The hypothesis here is that the one-dimensional morphology of CNTs and the two-dimensional morphology of GSs could form charge-transport efficient percolated networks if combined at the right proportions. Figure 11b shows the results of Pech-Pisté et al.^[43] on 1 wt% GS-CNT hybrid polysulfone nanocomposites. The CNTs used were as-received (not functionalized) MWCNTs of 1–6 μm length (mean 2.6 μm) and $\approx 110 \text{ m}^2 \text{ g}^{-1}$ specific surface area (measured by the Brunauer-Emmett-Teller, BET, method). The GSs are multilayer graphene sheets of 1–2.5 μm length (in-plane lateral size), not functionalized, and with a BET surface area of $\approx 183 \text{ m}^2 \text{ g}^{-1}$. ϕ_R in Figure 11b represents the ratio of the GS mass over the total filler (GS+CNT) mass. Thus $\phi_R = 0$ represents a nanocomposite with only CNTs. Composites with only GSs ($\phi_R = 1$) did not reach the required electrical conductivity for thermoresistive testing. This indicates that CNTs form a percolated network at lower filler concentrations than GSs, and reach higher conductivities at the same weight concentration. As seen from this figure, for this material system a hybrid made of 50% GSs and 50% CNTs by weight ($\phi_R = 0.50$) yields the highest thermoresistive sensitivity, but also higher hysteresis. On the other hand, including a smaller amount of GSs ($\phi_R = 0.25$, i.e., 25% GS and 75% CNTs) yields more modest increments of thermoresistive sensitivity, but without compromising the hysteresis.

7. Issues, Perspectives, and Concluding Remarks

The electrical response to temperature of a solid-state material serves as a unique fingerprint, offering insights into the charge

transport mechanisms taking place at the fundamental molecular level, with important applications in the sensing area. Smart materials can be designed and their sensitivity tailored by knowing the transduction function between the changes in electrical resistance and temperature, i.e., their thermoresistive response. The study of this thermoresistive response should include not only a broad range of temperatures (heating and cooling), but also its heating-cooling cyclic response. The study of the cyclic response would enable the assessment of hysteretic effects, which are crucial for accurately designing nanostructured sensors. Individual carbon nanostructures are the fundamental building blocks of engineering materials of larger scales (fibers, polymer composites), and their thermoresistive response needs to be further investigated. The study of the response of individual carbon nanostructures is technologically challenging, but it must be further pursued for a proper understanding of the fundamental quantum phenomena governing at such scale. For example, to fully understand the behavior of carbon nanotube (CNT) fibers and yarns, systematic hierarchical studies that cover individual CNTs, bundles, and fibers are necessary. Theoretical studies and computational modeling should of course aid in this task. The large majority of the thermoresistivity studies published focus on the application of a direct current electric field. It is expected that the electrical response to temperature under alternating current (AC) electric fields (thermoimpedance) provides valuable complementary information to further understand the governing phenomena. The AC alternative, however, has been only shallowly explored.

For polymer composites filled with carbon nanostructures, an important challenge to overcome is to build structure-property relationships between the micro- and nanostructure of the individual fillers (GS, CNTs) and the resulting thermoresistive response of the composite. Scientists need to be aware that to make this possible, detailed and reliable information on the physicochemical properties of the nanostructures needs to be included in the publications. For GSs and CNTs, the size distribution, number of layers, concentration and type of functional groups, interlayer spacing, and other relevant properties need to be accurately characterized and provided to build such structure-property relationships. Making a clear distinction between the different thermoresistive responses of materials of the graphene family requires their accurate identification and characterization at the nanostructure level. A major persisting issue is that many authors tend to ascribe the name “graphene” to any member of this broad family. Thus, adopting a proper and standardized nomenclature for members of the family of graphene (oxidized graphene, reduced graphene, few-layer graphene, multi-layer graphene, etc.) would greatly help the community to succeed in this task.

The use of hybrid fillers is an interesting path that demands further investigation. The intended use of hybrid fillers may be twofold, viz., to increase the thermoresistive sensitivity in temperature sensing applications, or to tailor the hybrid network for zero temperature sensitivity. On the one hand, an efficient thermoresistive network with sparse connections that readily reorganize under temperature is expected to increase the thermoresistive sensitivity. On the other hand, zero temperature coefficient of resistance materials are sought for non-temperature physical and chemical sensors, such as those for strain or moisture.

The primary applications of these carbon-nanostructured thermoresistive materials lie in the field of smart materials for sensing applications. They are expected to gear the next generation of temperature sensors, key components of soft robotics, tactile sensing, smart textiles, and wearable gadgets, among many others. In the form of fiber assemblies, they could be potentially used as an integral part of smart structural composites capable of self-sensing their temperature, and also for online polymer curing monitoring. In the field of robotics and automation, complex shapes of carbon-nanostructured polymer composites can be achieved by additive manufacturing, advancing toward a rapidly growing field known as “4D” printing. Combined with data-driven decision-making by machine learning strategies, and integrated with the internet of things, these smart materials are expected to confront the current and future challenges of sensory materials.

Appendix A

Table A1. Temperature coefficient of resistance of polymer composites filled with carbon nanotubes or graphenic sheets.

Filler	Matrix	Filler weight concentration [wt%]	Temperature Interval [°C]	α [% per °C]	Ref.
MWCNT	Epoxy	0.12	-40 to 110	0.97(@-40 °C) -0.91(@110 °C) (nl)	[35]
		3	-40 to 110	0.005(@-40 °C) -0.05(@110 °C) (nl)	
		5	-40 to 110	-0.35(@-40 °C) 0.49(@110 °C) (nl)	
MWCNT	Epoxy	0.1	50 to 200	-2.89 @50 °C (nl)	[119]
				-5.13 @80 °C (nl)	
				-8.98 @110 °C (nl)	
				-9.76 @140 °C (nl)	
				-7.56 @170 °C (nl)	
				3.3×10^{-2} @ 200 °C (nl)	
		5.0	50 to 200	0.66 @50 °C (nl)	
				-0.33 @80 °C (nl)	
				-2.14 @110 °C (nl)	
				-2.83 @140 °C (nl)	

(Continued)

Table A1. (Continued).

Filler	Matrix	Filler weight concentration [wt%]	Temperature Interval [°C]	α [% per °C]	Ref.
				-1.97@170 °C (nl)	
				32.9×10^{-3} @ 200 °C (nl)	
MWCNT	Epoxy	1	57 to 102	0.18 (c)	[34]
		3		1.40 (c)	
		5		2.6 (c)	
MWCNT	Epoxy	0.25	25 to 145	0.087(@104 °C) 0.35(@110 °C) (nl)	[9]
		0.50	25 to 145	0.045(@122 °C) (nl)	
MWCNT	Epoxy	0.05, 0.1, 0.3, 0.5	-130 to 75 (Fitting from -75 to 0)	-0.16 (c, nl)	[126]
MWCNT	Epoxy	0.5	0 to 80	-0.13	[127]
MWCNT	Epoxy	1.0	-20 to 80 (Fitting from -20 to 20 °C)	0.35 (c, nl)	[41]
		1.25		0.30 (c, nl)	
		1.75		0.14 (c, nl)	
		2.0		0.096 (c, nl)	
MWCNT	Epoxy	0.63	-20 to 60	-0.124	[130]
		1.25		-0.081	
		2.5		-0.070	
		5.0		-0.066	
MWCNT (aligned)	Epoxy	12	-95 to 100	-0.08 to -0.085	[134]
		57 to 60	-95 to 100	-0.135 to -0.154	
MWCNT	Polyester resin	0.1	-193 to 27 (Fitting from -173 °C to -73 °C)	-0.22 (c, nl)	[135]
		0.3		-0.20 (c)	
		0.5		-0.20 (c, nl)	
DWCNT	Polyester resin	0.1	-193 to 27 (Fitting from -173 °C to -73 °C)	-0.42 (c, nl)	
		0.3		-0.50 (c, nl)	
		0.5		-0.31 (c, nl)	
MWCNT	VER	0.1	40 to 160	-1.80×10^{-4} (@ 40 °C) -0.68×10^{-4} (@ 160 °C) (nl)	[47]

(Continued)

Table A1. (Continued).

Filler	Matrix	Filler weight concentration [wt%]	Temperature Interval [°C]	α [% per °C]	Ref.
		0.5		3.32×10^{-2} (@ 40 °C) -1.68×10^{-2} (@ 91 °C) 8.24×10^{-2} (@ 131 °C) (nl)	
		0.75		0.24 (@ 40 °C) -6.5×10^{-2} (@ 101 °C) 0.126 (@ 129 °C) (nl)	
		1.0		3.4×10^{-2} (@ 40 °C) -4.3×10^{-2} (@ 105 °C) 5.4×10^{-2} (@ 128 °C) (nl)	
MWCNT	VER	0.3	25 to 100	0.16 (nl)	[132]
			25 to -30	0.043 (nl)	
	PSF	1.0	25 to 100	0.29 (nl)	
			25 to -30	0.066 (nl)	
	PP	2.9	25 to 100	2.12 (nl)	
			25 to -30	0.159 (nl)	
MWCNT	PDMS	12	25 to 200 (Fitting from 79 to 200)	-0.17 (c, nl)	[136]
MWCNT	PDMS	2.0	25 to 50	7×10^{-4}	[137]
MWCNT	PEEK	10	20 to 140 (Fitting from 20 to 65)	-0.506 (c, nl)	[44]
MWCNT	PPR	4	37 to 100 (unconstrained)	-1.28	[138]
		4	37 to 100 (constrained)	-1.18	
		6	37 to 100 (unconstrained)	-0.66	
		6	37 to 100 (constrained)	-0.23	
		8	37 to 100 (unconstrained)	-1.07	
		8	37 to 100 (constrained)	-0.05	

(Continued)

Table A1. (Continued).

Filler	Matrix	Filler weight concentration [wt%]	Temperature Interval [°C]	α [% per °C]	Ref.
MWCNT	SEBS	16	20 to 60	-0.7	[139]
MWCNT	PI	1.2	0 to 125	-0.263	[46]
		1.4		-0.151	
		1.6		-0.175	
		1.8		-0.103	
		2.0		-0.147	
MWCNT	PSF	0.5	25 to 100	0.414	[42]
		1.0		0.191	
		5.0		0.213	
		10		0.194	
		25		0.06	
		40		-0.126	
		50		-0.304	
MWCNT	DAST	1.0	25 to 60	0.11	[120]
		6.7		-0.09	
SWCNT	PC	2.0	-73 to 73	-0.184	[140]
				(c)	
GS	PI	1.0	0 to 135	-0.366	[46]
		1.2		-0.313	
		1.4		-0.407	
		1.6		-0.207	
		1.8		-0.214	
GS	PI	4.0	25 to 80	-0.147 to -0.194	[129]
GS	PMMA	3.3 vol% 3.85 wt%* ($\rho_{PMMA} = 1.79 \text{ g/cm}^3$)	25 to 140	1.23 (@60 °C) 6.74 (@105 °C) (nl)	[48]
		3.8 vol.% 4.43 wt%* ($\rho_{PMMA} = 1.79 \text{ g/cm}^3$)		0.35 (@60 °C) 1.10 (@105 °C) (nl)	
		8.0 vol.% 9.26 wt%* ($\rho_{PMMA} = 1.79 \text{ g/cm}^3$)		0.11 (@60 °C) 0.54 (@105 °C) (nl)	
RGO	PCL	3.0	17 to 57	5.22 to 5.55	[141]
				(nl)	
		5.0	17 to 57	5.22 to 5.61	
				(nl)	
		7.0	17 to 57	5.26 to 5.63	
				(nl)	
RGO	CEL	5.0	7 to 107	-0.049	[142]
GS/ MWCNT (Hybrid)	PSF	1.0	25 to 100	0.09	[43]
		(25%GS/ 75%CNT)			
		1.0	25 to 100	0.166	
		(50%GS/ 50%CNT)			

(Continued)

Table A1. (Continued).

Filler	Matrix	Filler weight concentration [wt%]	Temperature Interval [°C]	α [% per °C]	Ref.
GS	PEVA (threads)	NR	25 to 40	0.368 (nl)	[143]
			20 to 40	-0.057 (annealed) (nl)	
Graphene nanowalls (380 nm height) on a polymer substrate	PDMS	N/A	25 to 45	1.14 (@25 °C) 20.0 (@45 °C)	[144]
	PET			-0.20 (@25 °C) -0.03 (@45 °C)	

CEL: Cellulose. DAST: 4-N,N-Dimethylamino-4'-N'-methyl-stilbazolium tosylate. DWCNT: Doublewall carbon nanotube. PC: Polycarbonate. PCL: Poly(ϵ -caprolactone). PDMS: Polydimethylsiloxane. PEEK: Poly ether ether ketone. PET: Poly(ethylene terephthalate). PEVA: Poly(ethylene-co-vinylacetate). PI: Polyimide. PMMA: Poly(methyl methacrylate). PP: Polypropylene. PPR: Polypropylene random copolymer. PSF: Polysulfone. RGO: Reduced graphene oxide. SEBS: Poly(styrene-*b*-(ethylene-co-butylene)-*b*-styrene). VER: Vinyl ester resin. N/A: Not applicable. NR: Not reported. ρ : density. (c): Calculated (estimated) from published plot or numerical data. (nl): Curve is nonlinear, a linear estimate was carried out. *Vol.% to wt% assumed $\rho_{GS} = 2.1 \text{ g/cm}^3$.

Acknowledgements

This review comprises research conducted by the author over several years, including funding from CONACYT (Mexico) and the Office of Naval Research Global (Award No. N62909-19-1-2119). The students who mainly contributed over the years to this topic are Marco Cen-Puc, Abraham Balam-Mena, and Raúl Pech-Pisté. Ignacio Isaac-Medina provided valuable assistance in updating the literature and calculating the TCRs. Dedicated assistance with literature search was diligently provided by Miriam Juan Qui-Valencia. Dr. Omar Rodríguez drew the artwork. The author is also thankful to Dr. Andres I. Oliva-Avilés and Dr. Juan V. Cauich-Rodríguez for proofreading. Special thanks go to Dr. Brenton Hammer for his kind invitation to this contribution.

Conflict of Interest

The author declares no conflict of interest.

Keywords

carbon nanostructures, carbon nanotubes, carbon nanotube yarns, graphene, nanocomposites, temperature coefficient of resistance, thermoresistivity

Received: March 14, 2023
Revised: July 4, 2023
Published online: August 16, 2023

[1] D. R. Askeland, P. P. Fulay, W. J. Wright, *The science and engineering of materials*, Cengage learning, Stamford, CT, USA 2010.

- [2] C. Kittel, P. McEuen, *Introduction to Solid State Physics*, John Wiley & Sons, Singapore **2018**.
- [3] T. W. Ebbesen, H. J. Lezec, H. Hiura, J. W. Bennett, H. F. Ghaemi, T. Thio, *Nature* **1996**, 382, 54.
- [4] P. Sun, M. Zhu, K. Wang, M. Zhong, J. Wei, D. Wu, H. Zhu, *ACS Appl. Mater. Interfaces* **2013**, 5, 9563.
- [5] S. Debroy, S. Sivasubramani, G. Vaidya, S. G. Acharyya, A. Acharyya, *Sci. Rep.* **2020**, 10, 6240.
- [6] A. Nag, R. B. V. B. Simorangkir, D. R. Gawade, S. Nuthalapati, J. L. Buckley, B. O'Flynn, M. E. Altinsoy, S. C. Mukhopadhyay, *Mater. Des.* **2022**, 221, 110971.
- [7] Q. Zheng, J. H. Lee, X. Shen, X. Chen, J. K. Kim, *Mater. Today* **2020**, 36, 158.
- [8] X. Zhang, S. Tang, R. Ma, Z. Chen, J. Zhuo, L. Cao, J. Yang, G. Yang, F. Yi, *Nano Energy* **2022**, 103, 107778.
- [9] H. Dai, E. T. Thostenson, T. Schumacher, *Composites, Part B* **2021**, 222, 109068.
- [10] B. C. Marin, S. E. Root, A. D. Urbina, E. Akilte, R. Miller, A. V. Zaretski, D. J. Lipomi, *ACS Omega* **2017**, 2, 626.
- [11] K. Chu, S. C. Lee, S. Lee, D. Kim, C. Moon, S. H. Park, *Nanoscale* **2015**, 7, 471.
- [12] G. Kuka, W. Kraak, H. J. Gollnest, R. Herrmann, *Phys. Status Solidi B* **1978**, 89, 547.
- [13] L. F. Mal'tseva, É. N. Marmer, *Soviet Powder Metall. Met. Ceram.* **1962**, 1, 34.
- [14] D. Destraz, L. Das, S. S. Tsirkin, Y. Xu, T. Neupert, J. Chang, A. Schilling, A. G. Grushin, J. Kohlbrecher, L. Keller, P. Puphal, E. Pomjakushina, J. S. White, *npj Quantum Mater.* **2020**, 5, 5.
- [15] E. Gati, S. L. Bud'ko, L. L. Wang, A. Valadkhani, R. Gupta, B. Kuthanazhi, L. Xiang, J. M. Wilde, A. Sapkota, Z. Guguchia, R. Khasanov, R. Valentí, P. C. Canfield, *Phys. Rev. B* **2021**, 104, 155124.
- [16] M. S. Fuhrer, J. Nygård, L. Shih, M. Forero, Y. G. Yoon, M. S. C. Mazzoni, H. J. Choi, J. Ihm, S. G. Louie, A. Zettl, P. L. McEuen, *Science* **2000**, 288, 494.
- [17] S. Mingiacchi, P. Lugli, A. Bonfiglio, G. Conte, M. Eickhoff, O. Ambacher, A. Rizzi, A. Passaseo, P. Visconti, R. Cingolani, *Phys. Status Solidi A* **2002**, 190, 281.
- [18] M. Ouyang, J. L. Huang, C. L. Cheung, C. M. Lieber, *Science* **2001**, 292, 702.
- [19] M. Dresselhaus, G. Dresselhaus, P. Eklund, *Science of Fullerenes and Carbon Nanotubes*, Academic Press, San Diego, CA, USA **1996**.
- [20] C. Villeneuve, S. Pacchini, P. Boulanger, A. Brouzes, F. Roussel, M. Pinault, M. Mayne-L'Hermite, R. Plana, *J. Appl. Phys.* **2012**, 112, 084327.
- [21] I. Stavarache, A. M. Lepadatu, V. S. Teodorescu, M. L. Ciurea, V. Iancu, M. Dragoman, G. Konstantinidis, R. Buiculescu, *Nanoscale Res. Lett.* **2011**, 6, 88.
- [22] Y. Tison, C. E. Giusca, V. Stolojan, Y. Hayashi, S. R. P. Silva, *Adv. Mater.* **2008**, 20, 189.
- [23] R. Saito, G. Dresselhaus, M. S. Dresselhaus, *J. Appl. Phys.* **1993**, 73, 494.
- [24] P. Delaney, M. Di Ventra, S. T. Pantelides, *Appl. Phys. Lett.* **1999**, 75, 3787.
- [25] B. Partoens, F. M. Peeters, *Phys. Rev. B* **2006**, 74, 075404.
- [26] N. F. Mott, *J. Non-Cryst. Solids* **1972**, 8–10, 1.
- [27] R. M. Hill, *Phys. Status Solidi A* **1976**, 34, 601.
- [28] Y. Yosida, I. Oguro, *J. Appl. Phys.* **1998**, 83, 4985.
- [29] X. Zhang, L. Yang, H. Liu, *Appl. Phys. Lett.* **2018**, 112, 164103.
- [30] Q. W. Li, Y. Li, X. F. Zhang, S. B. Chikkannanavar, Y. H. Zhao, A. M. Dangelewicz, L. X. Zheng, S. K. Doorn, Q. Jia, D. E. Peterson, P. N. Arendt, Y. Zhu, *Adv. Mater.* **2007**, 19, 3358.
- [31] P. Sheng, *Phys. Rev. B* **1980**, 21, 2180.
- [32] E. K. Sichel, P. Sheng, J. I. Gittleman, S. Bozowski, *Chin. Opt. Lett.* **1981**, 24, 6131.
- [33] H. Pang, Y. C. Zhang, T. Chen, B. Q. Zeng, Z. M. Li, *Appl. Phys. Lett.* **2010**, 96, 251907.
- [34] Alamusi, Y. Li, N. Hu, L. Wu, W. Yuan, X. Peng, B. Gu, C. Chang, Y. Liu, H. Ning, J. Li, Surina, S. A., H. Fukunaga, *Nanotechnology* **2013**, 24, 455501.
- [35] S. Gong, Y. Wang, Z. Xiao, Z. Li, Z. X. Wang, R. S. Lei, Z. H. Zhu, *Compos. Sci. Technol.* **2017**, 149, 48.
- [36] S. Gong, Z. H. Zhu, Z. Li, *Phys. Chem. Chem. Phys.* **2017**, 19, 5113.
- [37] M. Cen-Puc, A. I. Oliva-Avilés, F. Avilés, *Phys. E* **2018**, 95, 41.
- [38] B. F. Monea, E. I. Ionete, S. I. Spiridon, D. Ion-Ebrasu, E. Petre, *Sensors* **2019**, 19, 2464.
- [39] J. H. Lee, S. K. Kim, N. H. Kim, *Scr. Mater.* **2006**, 55, 1119.
- [40] M. O. Lisunova, Y. P. Mamunya, N. I. Lebovka, A. V. Melezhyk, *Eur. Polym. J.* **2007**, 43, 949.
- [41] N. T. Dinh, O. Kanoun, *Sensors* **2015**, 15, 11133.
- [42] M. Cen-Puc, G. Pool, A. I. Oliva-Avilés, A. May-Pat, F. Avilés, *Compos. Sci. Technol.* **2017**, 151, 34.
- [43] R. Pech-Pisté, M. Cen-Puc, A. Balam, A. May-Pat, F. Avilés, *Mater. Today Commun.* **2020**, 25, 101472.
- [44] M. Mohiuddin, S. V. Hoa, *Compos. Sci. Technol.* **2011**, 72, 21.
- [45] G. Matzeu, A. Pucci, S. Savi, M. Romanelli, F. Di Francesco, *Sens. Actuators A* **2012**, 178, 94.
- [46] Q. Li, S. Luo, Y. Wang, Q. M. Wang, *Sens. Actuators A* **2019**, 300, 111664.
- [47] K. L. Lasater, E. T. Thostenson, *Polymer* **2012**, 53, 5367.
- [48] X. Luo, D. W. Schubert, *Mater. Today Commun.* **2022**, 30, 103078.
- [49] A. Naeemi, J. D. Meindl, *IEEE Electron Device Lett.* **2007**, 28, 135.
- [50] L. Langer, V. V. Bayot, E. Grivei, J. Issi, J. P. Heremans, C. H. Olk, L. Stockman, C. Van Haesendonck, Y. Bruynseraede, *Phys. Rev. Lett.* **1996**, 76, 479.
- [51] C. L. Kane, E. J. Mele, R. S. Lee, J. E. Fischer, P. Petit, H. Dai, A. Thess, R. E. Smalley, A. R. M. Verschuere, S. J. Tans, C. Dekker, *Europhys. Lett.* **1998**, 41, 683.
- [52] V. Skákalová, A. B. Kaiser, Y. S. Woo, S. Roth, *Phys. Rev. B* **2006**, 74, 085403.
- [53] K. S. Novoselov, A. K. Geim, S. V. Morozov, D. Jiang, Y. Zhang, S. V. Dubonos, I. V. Grigorieva, A. A. Firsov, *Science* **2004**, 306, 666.
- [54] Q. Shao, G. Liu, D. Teweldebrhan, A. A. Balandin, *Appl. Phys. Lett.* **2008**, 92, 202108.
- [55] B. Davaji, H. D. Cho, M. Malakoutian, J. K. Lee, G. Panin, T. W. Kang, C. H. Lee, *Sci. Rep.* **2017**, 7, 8811.
- [56] K. Huang, J. Liu, L. Tan, J. Zuo, L. Fu, *Adv. Mater. Interfaces* **2018**, 5, 1701299.
- [57] D. Kong, L. T. Le, Y. Li, J. L. Zunino, W. Lee, *Langmuir* **2012**, 28, 13467.
- [58] B. Fang, J. Xi, Y. Liu, F. Guo, Z. Xu, W. Gao, D. Guo, P. Li, C. Gao, *Nanoscale* **2017**, 9, 12178.
- [59] W. F. W. Idris, N. F. A. Kasim, A. H. Abdullah, Z. A. Khusairi, K. Yusoh, Z. Ismail, *Ceram. Int.* **2020**, 46, 9176.
- [60] U. Sassi, R. Parret, S. Nanot, M. Bruna, S. Borini, D. De Fazio, Z. Zhao, E. Lidorikis, F. H. L. Koppens, A. C. Ferrari, A. Colli, *Nat. Commun.* **2017**, 8, 14311.
- [61] Y. Zeng, T. Li, Y. Yao, T. Li, L. Hu, A. Marconnet, *Adv. Funct. Mater.* **2019**, 29, 1901388.
- [62] G. García-Valdivieso, H. R. Navarro-Contreras, G. Vera-Reveles, F. J. González, T. J. Simmons, M. Gutiérrez Hernández, M. Quintana, J. G. Nieto Navarro, *Sens. Actuators, B* **2017**, 238, 880.
- [63] K. R. Reddy, S. Gandla, D. Gupta, *Adv. Mater. Interfaces* **2019**, 6, 1900409.
- [64] S. B. Subramanya, N. Nagarjuna, M. G. Anantha Prasad, M. M. Nayak, *Sens. Actuators A* **2019**, 295, 380.
- [65] S. Nuthalapati, V. Shirhatti, V. Kedambaimoole, N. V. Pandi, H. Takao, M. M. Nayak, K. Rajanna, *Sens. Actuators A* **2022**, 334, 113314.

- [66] M. Amjadi, M. Sitti, *Adv. Sci.* **2018**, *5*, 1800239.
- [67] E. P. Boon, L. T. Le, W. Y. Lee, *Carbon* **2016**, *102*, 81.
- [68] K. S. Karimov, M. T. S. Chani, F. A. Khalid, *Phys. E* **2011**, *43*, 1701.
- [69] S. Selvarasah, A. Busnaina, M. R. Dokmeci, *IEEE Trans. Nanotechnol.* **2011**, *10*, 13.
- [70] M. Mahjouri-Samani, Y. S. Zhou, X. N. He, W. Xiong, P. Hilger, Y. F. Lu, *Nanotechnology* **2013**, *24*, 035502.
- [71] I. Banerjee, T. Faris, Z. Stoeva, A. K. Sharma, A. K. Ray, *Mater Today Proc* **2016**, *3*, 4035.
- [72] S. Lu, C. Zhao, L. Zhang, D. Chen, D. Chen, X. Wang, K. Ma, *RSC Adv.* **2018**, *8*, 22078.
- [73] S. Sibilia, F. Bertocchi, S. Chiodini, F. Cristiano, L. Ferrigno, G. Giovinco, A. Maffucci, *Nanotechnology* **2021**, *32*, 275701.
- [74] J. Štulík, O. Musil, F. Josefík, P. Kadlec, *Nanomaterials* **2022**, *12*, 1594.
- [75] G. T. Kim, S. H. Jhang, J. G. Park, Y. W. Park, S. Roth, *Synth. Met.* **2001**, *117*, 123.
- [76] F. Avilés, A. I. Oliva-Avilés, M. Cen-Puc, *Adv. Eng. Mater.* **2018**, *20*, 1701159.
- [77] A. Buldum, J. P. Lu, *Phys. Rev. B* **2001**, *63*, 161403.
- [78] A. Allaoui, S. V. Ho, P. Evesque, J. Bai, *Scr. Mater.* **2009**, *61*, 628.
- [79] J. G. Simmons, *J. Appl. Phys.* **1963**, *34*, 2581.
- [80] J. G. Simmons, *J. Appl. Phys.* **1963**, *34*, 1793.
- [81] C. Li, E. T. Thostenson, T. W. Chou, *Appl. Phys. Lett.* **2007**, *91*, 223114.
- [82] R. Rahman, P. Servati, *Nanotechnology* **2012**, *23*, 055703.
- [83] R. Bai, Y. Gao, C. Lu, J. Tan, F. Xuan, *Measurement* **2021**, *169*, 108348.
- [84] V. S. Turkani, D. Maddipatla, B. B. Narakathu, B. J. Bazuin, M. Z. Atashbar, *Sens. Actuators A* **2018**, *279*, 1.
- [85] S. Kanaparthi, S. Badhulika, *Nanotechnology* **2016**, *27*, 095206.
- [86] M. A. Cullinan, R. M. Panas, M. L. Culpepper, *Nanotechnology* **2012**, *23*, 325501.
- [87] D. Janas, K. K. K. Koziol, *Appl. Surf. Sci.* **2016**, *376*, 74.
- [88] D. Jung, D. Kim, K. H. Lee, L. J. Overzet, G. S. Lee, *Sens. Actuators A* **2013**, *199*, 176.
- [89] C. Christianson, R. Lu, J. Wu, *Nanotechnology* **2014**, *25*, 425503.
- [90] J. G. Park, N. G. Yun, Y. B. Park, R. Liang, L. Lumata, J. S. Brooks, C. Zhang, B. Wang, *Carbon* **2010**, *48*, 4276.
- [91] A. Maffucci, F. Micciulla, A. E. Cataldo, G. Miano, S. Bellucci, *IEEE Trans. Compon., Packag., Manuf. Technol.* **2017**, *7*, 485.
- [92] C. K. M. Fung, V. T. S. Wong, R. H. M. Chan, W. J. Li, *IEEE Trans. Nanotechnol.* **2004**, *3*, 395.
- [93] K. Kędzierski, K. Rytel, Ł. Majchrzycki, D. Wróbel, *Thin Solid Films* **2015**, *589*, 701.
- [94] J. Park, I. R. Jang, K. Lee, H. J. Kim, *Sensors* **2019**, *19*, 3878.
- [95] R. Kumar, M. A. Khan, A. V. Anupama, S. B. Krupanidhi, B. Sahoo, *Appl. Surf. Sci.* **2021**, *538*, 148187.
- [96] S. Lu, D. Chen, X. Wang, J. Shao, K. Ma, L. Zhang, S. Araby, Q. Meng, *Compos. Sci. Technol.* **2017**, *152*, 181.
- [97] A. Di Bartolomeo, M. Sarno, F. Giubileo, C. Altavilla, L. Lemmo, S. Piano, F. Bobba, M. Longobardi, A. Scarfato, D. Sannino, A. M. Cucolo, P. Ciambelli, *J. Appl. Phys.* **2009**, *105*, 064518.
- [98] M. I. Ionescu, Y. Zhang, R. Li, H. Abou-Rachid, X. Sun, *Appl. Surf. Sci.* **2012**, *258*, 4563.
- [99] S. Völlebregt, R. Ishihara, *Carbon* **2016**, *96*, 332.
- [100] J. Liu, C. Cai, H. Liang, *Chin. Opt. Lett.* **2012**, *10*, S23101.
- [101] S. Gong, D. Wu, Y. Li, M. Jin, T. Xiao, Y. Wang, Z. Xiao, Z. Zhenghong, Z. Li, *Carbon* **2018**, *137*, 188.
- [102] M. Zhang, K. R. Atkinson, R. H. Baughman, *Science* **2004**, *306*, 1358.
- [103] A. Mikhalchan, C. Madrona, L. Arévalo, M. Malfois, J. J. Vilatela, *Carbon* **2022**, *197*, 368.
- [104] A. Can-Ortiz, J. L. Abot, F. Avilés, *Carbon* **2019**, *145*, 119.
- [105] C. Pérez-Aranda, R. Pech-Pisté, H. J. Carrillo-Escalante, G. C. Uribe-Riestra, F. Avilés, *J Eng Mater Technol* **2023**, *145*, 011005.
- [106] B. Nysten, J. P. Issi, R. Barton Jr, D. R. Boyington, J. G. Lavin, *J. Phys. D: Appl. Phys.* **1991**, *24*, 714.
- [107] A. Lekawa-Raus, K. Walczak, G. Kozłowski, M. Wozniak, S. C. Hopkins, K. K. Koziol, *Carbon* **2015**, *84*, 118.
- [108] J. F. Niven, M. B. Johnson, S. M. Juckes, M. A. White, N. T. Alvarez, V. Shanov, *Carbon* **2016**, *99*, 485.
- [109] A. E. Aliev, C. Guthy, M. Zhang, S. Fang, A. A. Zakhidov, J. E. Fischer, R. H. Baughman, *Carbon* **2007**, *45*, 2880.
- [110] A. Balam, M. Cen-Puc, O. Rodríguez-Uicab, J. L. Abot, F. Avilés, *Adv. Eng. Mater.* **2020**, *22*, 2000220.
- [111] V. T. Dau, C. D. Tran, T. T. Bui, V. D. X. Nguyen, T. X. Dinh, *RSC Adv.* **2016**, *6*, 106090.
- [112] M. Han, Y. Bang, W. Kim, G. S. Lee, D. Jung, *Microelectron. Eng.* **2017**, *168*, 50.
- [113] T. Dinh, H. P. Phan, T. K. Nguyen, A. Qamar, A. R. M. Foisal, N. T. Viet, C. D. Tran, Y. Zhu, N. T. Nguyen, D. V. Dao, *J. Mater. Chem. C* **2016**, *4*, 10061.
- [114] Y. Wada, K. Kita, K. Takei, T. Arie, S. Akita, *Appl. Phys. Express* **2016**, *9*, 085001.
- [115] O. Rodríguez-Uicab, J. L. Abot, F. Avilés, *Sensors* **2020**, *20*, 3230.
- [116] O. Rodríguez-Uicab, I. Guay, J. L. Abot, F. Avilés, *Polymers* **2021**, *13*, 783.
- [117] M. Haghgoo, R. Ansari, M. K. Hassanzadeh-Aghdam, L. Tian, M. Nankali, *Composites, Part A* **2022**, *163*, 107244.
- [118] M. Haghgoo, R. Ansari, M. K. Hassanzadeh-Aghdam, M. Nankali, *Acta Mater.* **2022**, *230*, 117870.
- [119] T. Xiao, S. Gong, X. Lei, Z. Jiang, Y. Wang, D. Wu, Z. Xiao, Z. Zhu, Z. Li, *Compos. Sci. Technol.* **2018**, *167*, 563.
- [120] X. Xu, L. Huang, K. Fan, Y. Jiang, Z. Sun, Q. He, T. Ao, R. Huang, Y. Wen, C. Ma, *J. Mater. Chem. C* **2014**, *2*, 2394.
- [121] W. Gao, Z. Zhang, Y. Zhang, B. Ma, J. Luo, J. Deng, W. Yuan, *Compos. Sci. Technol.* **2020**, *199*, 108333.
- [122] R. Zhang, M. Baxendale, T. Peijs, *Phys. Rev. B* **2007**, *76*, 195433.
- [123] Y. Zeng, G. Lu, H. Wang, J. Du, Z. Ying, C. Liu, *Sci. Rep.* **2014**, *4*, 6684.
- [124] S. E. Lee, Y. Sohn, K. Chu, D. Kim, S. H. Park, M. Bae, D. Kim, Y. Kim, I. Han, H. J. Kim, *Org. Electron.* **2016**, *37*, 371.
- [125] I. Pérez, S. Flores, C. Ortiz, M. Rivero, J. E. Corona, A. I. Oliva, F. Avilés, *Polym. Compos.* **2022**, *43*, 2150.
- [126] J. T. Shen, S. T. Buschhorn, J. T.h.M. D.e Hosson, K. Schulte, B. Fiedler, *Compos. Sci. Technol.* **2015**, *115*, 1.
- [127] A. Sanli, A. Benchirouf, C. Müller, O. Kanoun, *Sens. Actuators A* **2017**, *254*, 61.
- [128] S. Zhao, D. Lou, P. Zhan, G. Li, K. Dai, J. Guo, G. Zheng, C. Liu, C. Shen, Z. Guo, *J. Mater. Chem. C* **2017**, *5*, 8233.
- [129] Y. Jiang, M. Liu, X. Yan, T. Ono, L. Feng, J. Cai, D. Zhang, *Adv. Mater. Technol.* **2018**, *3*, 1800113.
- [130] S. J. Lee, Y. J. Jung, J. Park, S. H. Jang, *Nanomaterials* **2022**, *12*, 2369.
- [131] S. C. Tjong, G. B. Liang, S. P. Bao, *Scr. Mater.* **2007**, *57*, 461.
- [132] A. Balam, M. Cen-Puc, A. May-Pat, J. L. Abot, F. Avilés, *Smart Mater. Struct.* **2019**, *29*, 015012.
- [133] M. Haghgoo, R. Ansari, S. H. Jang, M. K. Hassanzadeh-Aghdam, M. Nankali, *Composites, Part A* **2023**, *166*, 107380.
- [134] M. Mecklenburg, D. Mizushima, N. Ohtake, W. Bauhofer, B. Fiedler, K. Schulte, *Carbon* **2015**, *91*, 275.
- [135] Y. Simsek, L. Ozyuzer, A. T. Seyhan, M. Tanoglu, K. Schulte, *J. Mater. Sci.* **2007**, *42*, 9689.
- [136] K. Chu, S. H. Park, *IEEE Electron Device Lett.* **2015**, *36*, 50.
- [137] S. Pyo, J. I. Lee, M. O. Kim, T. Chung, Y. Oh, S. C. Lim, J. Park, J. Kim, *J. Micromech. Microeng.* **2014**, *24*, 075012.
- [138] P. Verma, A. Schiffer, S. Kumar, *Polym. Test.* **2021**, *93*, 106961.
- [139] N. Calisi, A. Giuliani, M. Alderighi, J. M. Schnorr, T. M. Swager, F. Di Francesco, A. Pucci, *Eur. Polym. J.* **2013**, *49*, 1471.
- [140] A. E. Aliev, *Infrared Phys. Technol.* **2008**, *51*, 541.

- [141] P. X. Thinh, C. Basavajara, J. K. Kim, D. S. Huh, *Polym. Compos.* **2012**, 33, 2159.
- [142] Y. Chen, P. Pötschke, J. Pionteck, B. Voit, H. Qi, *J. Mater. Chem. A* **2018**, 6, 7777.
- [143] S. V. Patel, S. Cemalovic, W. K. Tolley, S. T. Hobson, R. Anderson, B. Fruhberger, *ACS Sens.* **2018**, 3, 640.
- [144] H. Zhang, K. Zhao, S. Cui, J. Yang, D. Zhou, L. Tang, J. Shen, S. Feng, W. Zhang, Y. Fu, *Nanophotonics* **2018**, 7, 883.



Francis Avilés is a Senior Scientist at the Materials Department of the “Scientific Research Center of Yucatan” (CICY for its Spanish acronym), located in Mérida, Mexico. He is a Mechanical Engineer with a Master’s degree in Applied Physics and a PhD in solid body mechanics from Florida Atlantic University. He worked as a Research Associate at the Center for Composite Materials of the University of Delaware. He has published more than 130 journal papers with over 3,200 citations. His current research interests focus on the electro-mechanics, piezoresistive, thermoresistive, and multifunctional properties of nanostructured polymer composites, carbon nanostructures, and smart materials.